UDC 666.762.11.046.512.032.5

SYNTHESIS AND PROPERTIES OF FUSION-CAST REFRACTORIES IN THE $Al_2O_3 – ZrO_2$ SYSTEM

V. A. Sokolov[1] and M. D. Gasparyan[1]

Translated from Novye Ogneupory, No. 3, pp. 39 – 43, March, 2004.

The synthesis and properties of fusion-cast refractories in the $Al_2O_3 – ZrO_2$ system studied by x-ray phase analysis and petrography are reported. The phase composition of synthetic materials is represented by corundum and ZrO_2 monoclinic modification. Adding ZrO_2 results in a decrease in the size of corundum crystals. The corrosion resistance of the synthetic refractories increases with ZrO_2 concentration; still, further effort is needed to improve the fabricability of fusion-cast $Al_2O_3 – ZrO_2$-based refractories.

The $Al_2O_3 – ZrO_2$ system, owing to the high melting point, corrosion resistance, and hardness of its constituent components, has been and continues to be an object of studies focused on the development of refractory and abrasive materials. The system in question has no other chemical species; however, it displays a eutectic whose composition, judging from the literature, remains a debatable issue. According to data reported in [1], the eutectic has a melting point in the range of 1885 to 1920°C and contains 32 to 55% ZrO_2. The $Al_2O_3 – ZrO_2$ system has been studied in detail in [2] using methods of high-temperature x-ray diffractometry and petrography and was found to have eutectic temperature and composition 1910 ± 20°C and 42.5 ± 1 wt.% ZrO_2. These results (Fig. 1) are in good agreement with the composition diagram reported in [3]. To our knowledge, little (if any) was reported in the literature concerning the preparation of fusion-cast refractory materials and their technological implications. Most studies were concerned with granular materials derived from sprayed melts or small-sized specimens [4 – 6]; in contrast, our goal was to synthesize materials in the $Al_2O_3 – ZrO_2$ system, to prepare large-sized castings, and to determine their physicomechanical and performance characteristics. Compositionally, the synthesized materials were confined within 60% ZrO_2, that is, a region containing eutectic species.

To prepare mixtures for the synthesis, G-1-grade alumina (State Standard GOST 6912–87) and TsrO-1-grade zirconia were used. The mixtures were melted in an arc furnace powered from a 430 kV · A transformer. The molten material was poured in molds with inside dimensions of $175 \times 250 \times 300$ mm composed of graphite plates. The molded castings (ingots) were annealed under natural conditions in a thermal box under a layer of heat-insulating pack; after weighing and measuring, the ingots were cut with a diamond tool lengthwise for inspection and structural analysis. The ingots are shown in Fig. 2; relevant characteristics are given in Table 1.

The ingots displayed cracks, streaks and spallings, which indicates poor fabricability. Ingots with 2 – 5% ZrO_2 (P-285 and P-286) in appearance did not differ much from the corundum-based zirconia-free ingot P-275. The ingots displayed a multiple gas porosity because of the bulk crystallization; the introduction of ZrO_2 into the mixture resulted in a slight densification. Material with 10% ZrO_2 (P-303) showed a somewhat more dense and uniform texture. Further in-

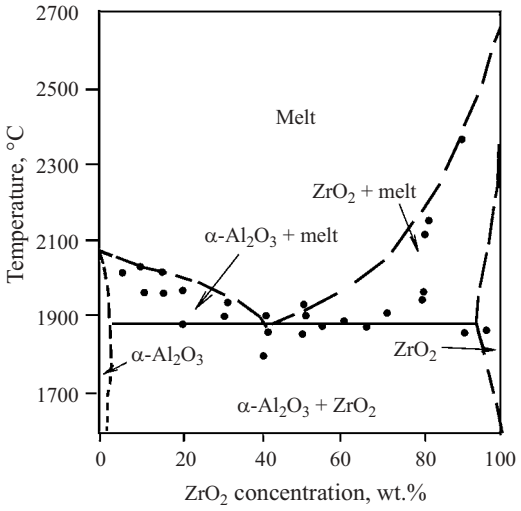

Fig. 1. $Al_2O_3 – ZrO_2$ composition diagram [2].

[1] Moscow Institute for Steel and Alloys, Moscow, Russia; SpetsPromOgneupor Joint-Stock Co., Russia.

1083-4877/04/4503-0210 © 2004 Plenum Publishing Corporation

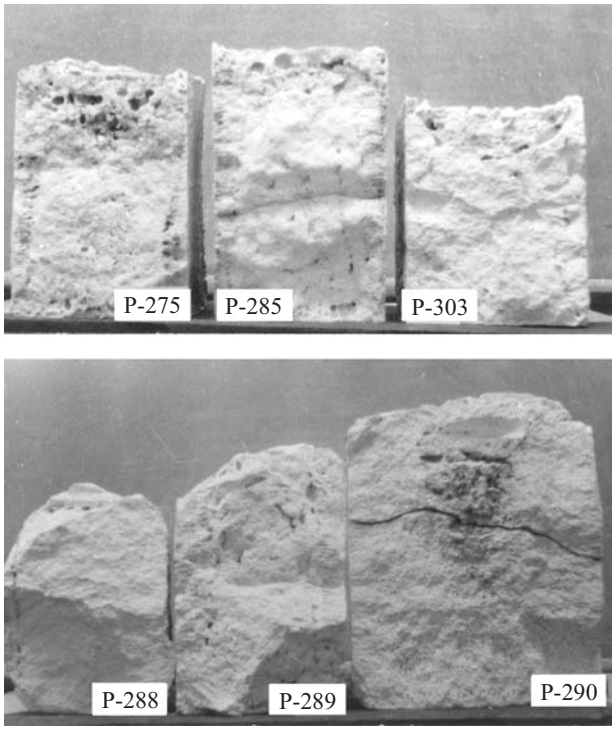

Fig. 2. Ingots of synthetic refractory materials.

crease in ZrO_2 concentration produced little improvement to the texture properties. Virtually all ingots displayed a multiple gas porosity and an indistinct shrinkage cavity. A clearly defined shrinkage cavity could be observed only in ingot P-290 of post-eutectic composition.

The phase composition of materials was studied using x-ray diffractometry and petrography analysis. Typical x-ray diffraction patterns are presented in Fig. 3. The phases were identified with reference to the ASTM Powder Diffraction File [7]. The crystal phases in synthetic materials were found to be corundum and monoclinic zirconia.

The x-ray diffraction pattern of a specimen with 5% ZrO_2 shows intense peaks characteristic of α-Al_2O_3 (3.48, 2.557, 2.386, 2.090, 1.752, and 1.605 Å) and peaks of lesser

TABLE 1. Characterization of Molded Synthetic Materials

Material	Composition, wt.%		Ingot characteristics			
	Al_2O_3	ZrO_2	weight, kg	dimensions, mm	apparent density,* g/cm^3	open porosity,* %
P-285	98.2	2.0	33.3	175 × 250 × 270	3.34	8.2
P-286	95.0	5.0	27.0	175 × 250 × 190	3.45	7.0
P-303	90.0	10.0	29.6	175 × 250 × 220	3.54	5.9
P-288	80.0	20.0	38.3	175 × 250 × 250	3.61	9.4
P-289	60.0	40.0	39.7	175 × 250 × 270	3.74	8.3
P-290	40.0	60.0	46.6	175 × 250 × 290	3.85	9.2

* Measured on specimens cut out of the working zone of an ingot.

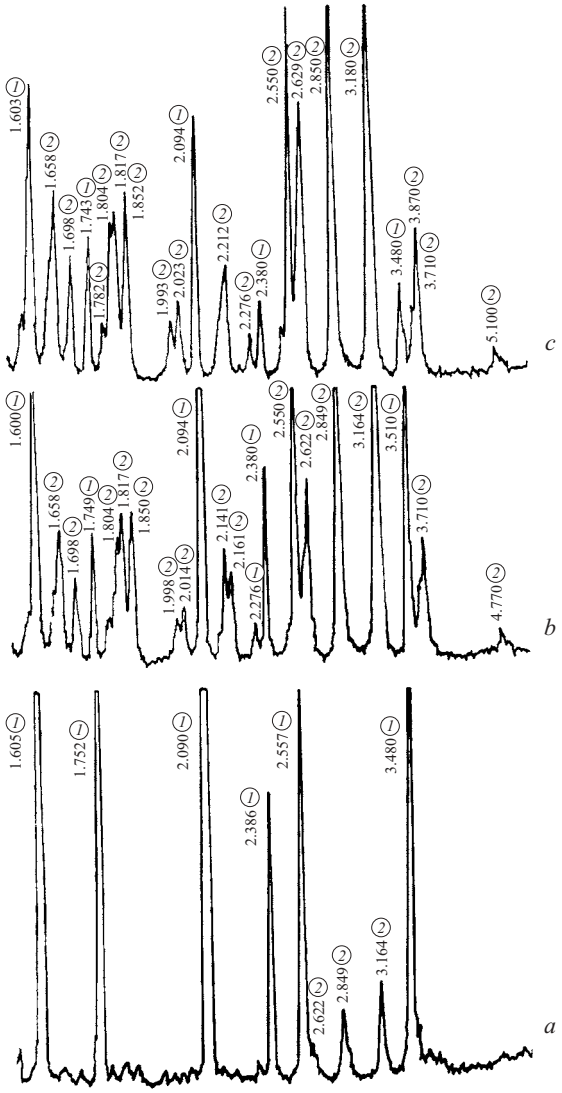

Fig. 3. X-ray diffraction patterns of fused refractories in the $Al_2O_3 – ZrO_2$ system: *a*) P-286; *b*) P-289; *c*) P-290; *1*) α-Al_2O_3; *2*) ZrO_2 (monocl.).

intensity of monoclinic ZrO_2 (3.164, 2.849, and 2.622 Å). The latter peaks (characteristic of baddeleyite) gradually gain in intensity with increase in ZrO_2 concentration in the refractory and new features appear (4.77, 3.71, 2.161, 2.141, 1.85, 1.658 Å, etc.); these reach a maximum in specimen with 60% ZrO_2 (P-290).

The petrographic analysis was carried out on a Neophot-21 microscope; typical photomicrographs are shown in Fig. 4.

Specimen P-285 (2% ZrO_2) features isometric corundum grains, predominantly of square shape, 0.05 to 0.3 mm across (on average, 0.15 mm). Its picture shows microcracks and multiple pores confined to the corundum grain boundaries. Occasionally, baddeleyite segregations could be seen as thin interlayers (about 0.003 mm) sandwiched between corundum grains. Presumably, most baddeleyite is “lost” in intergranu-

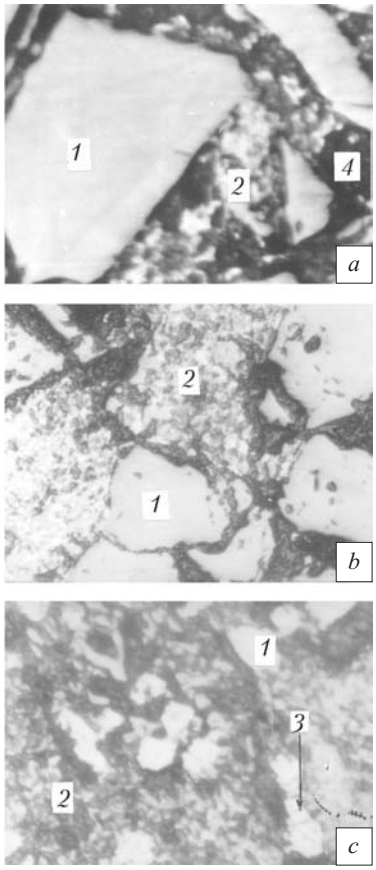

Fig. 4. Photomicrographs of synthetic fusion-cast materials P-303 (*a*), P-288 (*b*), and P-290 (*c*): *1*) corundum; *2*) co-crystallized corundum and baddeleyite; *3*) baddeleyite; *4*) pores. × 300 (viewed in reflected light).

lar cracks. As the ZrO_2 concentration increases to 5% ZrO_2 (P-286), the corundum grain size tends to decrease somewhat to 0.03 – 0.15 mm (mainly to 0.08 mm). Baddeleyite is present in minor amounts (less than 5%) seen as thin interlayers between corundum grains.

Specimen P-303 (10% ZrO_2) shows a fine- and medium-size grain structure with the predominance of corundum phase seen as isometric grains 0.03 – 0.1 mm across (0.07 mm on average). In places, larger crystals are observed, however, not exceeding 0.2 mm (Fig. 4*a*). Corundum mostly occurs in the form of intergrown aggregates; occasionally, the grains are separated by co-crystallized interlayers of corundum and baddeleyite.

Its mineral composition is about 90% corundum and 10% co-crystallized corundum and baddeleyite. The thin section surface shows a network of fine cracks, mainly confined to the corundum grain boundaries. Characteristically, in corundum grains that are in contact with each other through a co-crystallized corundum + baddeleyite interlayer, no cracks were observed.

P-288 specimen (20% ZrO_2) has a fine-grained panidiomorphic structure (that is, a structure with a varying degree of isomorphism of its elements) composed of corundum and co-crystallized eutectic of corundum and baddeleyite (Fig. 4*b*). The majority of corundum grains exhibit an isometric idiomorphic shape. The corundum grains are 0.02 – 0.10 mm across (0.08 mm on average). The space between grains is filled with corundum and baddeleyite produced during the eutectic co-crystallization. The textural pattern is mainly formed by self-crystallized corundum grains. Corundum is the controlling phase in the process of joint (eutectic) crystallization. Baddeleyite is seen as point-like or slender elongate clusters embedded in the corundum matrix. Other conspicuous structural features are rather large (up to 0.01 mm) grains of self-crystallized baddeleyite. The phase composition is: 60 – 65% corundum and 35 – 40% co-crystallized corundum and baddeleyite. The texture of the material is porous, showing irregularly shaped pores up to 0.2 mm across confined to the boundaries of structural elements; the pores account for about 10% of the total surface of the thin section.

Specimen P-289 (40% ZrO_2) differs from the previous specimen in the somewhat smaller number and smaller size of corundum grains (average 0.06 mm across) and in the larger amount of another structural components – eutectic intergrown crystals of corundum and baddeleyite. The mineral composition consists of 40 – 45% corundum and 55 – 60% of intergrown crystals of corundum and baddeleyite. The pores are irregularly shaped and account for 5 – 8% of the total surface of the thin section.

In specimen P-290 (60% ZrO_2), the predominant phase is represented by eutectic intergrown crystalline grains of corundum and baddeleyite (Fig. 4*c*). Characteristically, the central grain zone is rich in baddeleyite, whereas corundum is predominant in the peripheral zone. The grains are intimately intergrown, and the dividing boundary between them can be drawn only arbitrarily either guided by the different orientation of baddeleyite moieties embedded in the corundum matrix, or by the peripheral zone of predominantly corundum composition. The average size of eutectic grains is about 0.1 mm across. The self-crystallized baddeleyite shows a very irregular distribution and occurs as isometric grains about 0.015 mm across with a tortuous boundary line. The baddeleyite grains form spatial bridges with single, mainly skeletal, corundum about 0.01 mm across with a clear crystallographic contour. The material exhibits a crack-like texture. Some pores (total less than 5%) reach 0.8 mm in size.

The synthetic materials were tested for corrosion resistance using molten industrial glasses: sodium-calcium silicate sheet glass, crystal glass, electron-tube glass, and S52-1-grade borosilicate glass. The tests were carried out under static conditions at 1400 – 1450°C and holding times from 24 to 40 h. The corrosion resistance was evaluated by measuring the change in linear dimensions of the specimens placed afloat in the molten glass. Relevant results are summarized in Table 2; the appearance of tested specimens is shown in Fig. 5. For comparison, parallel tests were carried

TABLE 2. Corrosion Resistance of Fusion-Cast Materials in the $Al_2O_3 – ZrO_2$ System

Material	Corrosion rate, mm/day, tested by molten glass*			
	Na – Ca silicate glass (1450°C, 40 h)	S52-1 borosilicate glass (1450°C, 30 h)	electron-tube glass (1400°C, 30 h)	crystal glass (1450°C, 24 h)
Experimental specimens:				
P-275	2.00	0.45	0.20	0.80
P-286	1.15	Not determ.	Not determ.	0.55
P-303	Not determ.	0.30	0.15	Not determ.
P-288	0.85	Not determ.	0.10	0.40
P-289	0.45	0.25	0.10	0.10
P-290	0.35		Not determ.	
KÉL-95	1.90	0.65	0.20	0.70
Monofrax M	0.85	0.55	0.20	0.45
Jargal M	Not determ.	0.50		
ER 1681	0.25	0.40	0.10	0.20

* Data in brackets refer to testing temperature and holding time.

out using standard industrial fusion-cast refractories of grades KÉL-95, Monofrax M, Jargal M, and ER 1681.

The corrosion resistance of synthetic materials was found to increase with ZrO_2 concentration. P-303 specimen (10% ZrO_2) tested by S52-1 borosilicate glass and electron-tube glass showed a corrosion resistance superior to that of the industrial alumina refractories KÉL-95 and Monofrax M; when tested by the molten electron-tube glass, their corrosion resistance was roughly the same. Further increase in ZrO_2 concentration makes the synthetic refractory more resistant to molten electron-tube glass. The refractory containing 20% ZrO_2 shows resistance to the corrosion attack of molten Na – Ca silicate sheet and crystal glasses similarly to Monofrax M and Jargal M.

Thus the results of our study show that adding ZrO_2 to refractories increases their corrosion resistance to molten industrial glasses. Another benefit is the reduction in size of corundum crystals in the structure of synthetic materials. Still, the fabricability of ingots derived from the two-component system $Al_2O_3 – ZrO_2$ is insufficient and more effort is needed to make the refractory material less prone to cracking.

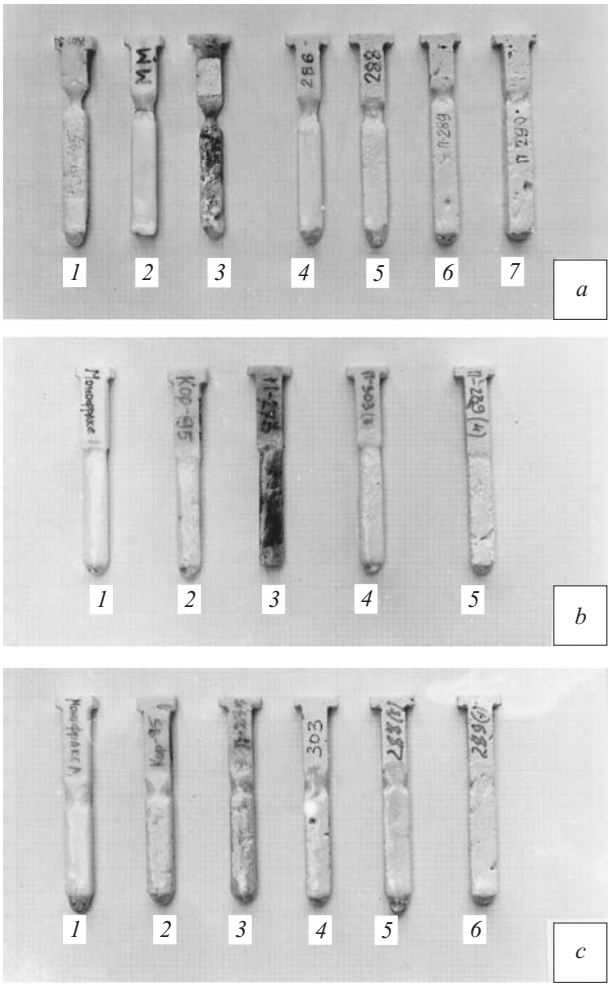

Fig. 5. Specimens of fusion-cast refractories tested for corrosion resistance using molten glasses: *a*) Na – Ca silicate glass, refractories KÉL-95 (*1*), Monofrax M (*2*), P-275 (*3*), P-286 (*4*), P-288 (*5*), P-289 (*6*), P-290 (*7*); *b*) S52-1 borosilicate glass, refractories Monofrax M (*1*), KÉL-95 (*2*), P-275 (*3*), P-303 (*4*), P-289 (*5*); *c*) electron-tube glass, refractories Monofrax M (*1*), KÉL-95 (*2*), P-275 (*3*), P-303 (*4*), P-288 (*5*); P-289 (*6*).

REFERENCES

1. A. S. Berezhnoi, *Multicomponent Oxide Systems* [in Russian], Naukova Dumka, Kiev (1970).
2. G. R. Fisher, L. J. Manfredo, R. N. McNally, and R. C. Doman, "The eutectic and liquidus in the $Al_2O_3 – ZrO_2$ system," *J. Mater. Sci.*, **16**(12), 3447 – 3451 (1981).
3. A. M. Alper, "Phase diagrams," *Mater. Sci. Tech.*, **11**, 130 (1970).
4. N. Clausen, G. Lindemann, and G. Petrow, "Rapid solidification in the $Al_2O_3 – ZrO_2$ system," *Ceram. Int.*, **9**(3), 83 – 86 (1983).
5. S. Ambalavanan, M. P. Gunasekar, and M. Sundaram, "Evaluation of microstructure and hardness of fused zirconia – alumina for abrasive applications," *Bull. Electrochem.*, **2**(1), 45 – 57 (1986).
6. V. A. Kryuchkov, L. P. Ivanova, A. V. Galakhov, et al., "$Al_2O_3 – ZrO_2$ ceramics from powders derived from the melt by high-speed solidification," *Ogneupory*, No. 6, 19 – 22 (1989).
7. *Inorganic Index to the Powder Diffraction File*, ASTM (1967).